A Method for Improved VCSEL Packaging Using MEMS and Ink-Jet Technologies

Arun Kumar Nallani, Ting Chen, *Member, IEEE*, Donald J. Hayes, Woo-Seong Che, and Jeong-Bong Lee, *Member, IEEE*

***Abstract*—Vertical-cavity surface-emitting lasers (VCSELs) have been recognized as low-cost low-power light sources for applications, such as, optoelectronic (OE) interconnects for high-speed optical data communication. However, many VCSEL applications have not been fully realized due to the lack of solutions to technical issues such as optical coupling, alignment, interconnects, and RF compatibility. In this paper, the authors propose microelectromechanical systems (MEMS) and MEMS-enabled ink-jet printing technologies to provide improved solutions to these technically challenging problems in OE-device packaging. Wafer-level microoptical elements consisting of transparent polymeric pedestals and microlenses were designed and fabricated directly on top of the VCSEL-emitting facets to improve the optical-coupling efficiency between the VCSEL and the optical fiber. Self-aligning MEMS clampers and micromold structures were designed and fabricated for precise packaging and reliable electrical connection of diced VCSEL arrays. This novel packaging process is substrate independent and relatively simple. This technique will provide a reliable assembly of OE devices in miniature optical systems on various substrates.**

***Index Terms*—Ink-jet printing, microelectromechanical systems (MEMS), optoelectronic (OE), packaging, vertical-cavity surface-emitting laser (VCSEL).**

I. Introduction

VERTICAL-CAVITY surface-emitting lasers (VCSELs) have been well recognized as low-cost low-power light sources for advanced optoelectronic (OE) interconnects developed for parallel high-bandwidth high-density optical data communication, network switching, and signal processing [1]–[3]. However, this technology has not been fully commercially realized due to problems such as optical coupling and alignment [4], [5], electrical interconnects [4], [6], RF compatibility [7], [8], and thermal management [9].

Manuscript received February 17, 2005; revised July 8, 2005. This work was supported in part by the National Institute of Standards and Technology-Advanced Technology Program (NIST-ATP) under Grant 70NANB1H3021 and in part by the National Science Foundation (NSF) Small Business Innovation Research (SBIR) Program under Grant DMI-0214924.

A. K. Nallani is with the University of Texas at Dallas (UTD), Richardson, TX 75080 USA, and also with MicroFab Technologies, Plano, TX 75074 USA (e-mail: acn016100@utdallas.edu).

T. Chen and D. J. Hayes are with MicroFab Technologies, Plano, TX 75074 USA (e-mail: tchen@microfab.com; dhayes@microfab.com).

W.-S. Che was with University of Texas at Dallas (UTD), Richardson, TX 75080 USA. He is now with Tongmyung University of Information Technology, Busan 608711, Korea (e-mail: wsche@tit.ac.kr).

J.-B. Lee is with University of Texas at Dallas (UTD), Richardson, TX 75080 USA (e-mail: jblee@utdallas.edu).

Digital Object Identifier 10.1109/JLT.2005.863305

A popular method of packaging VCSELs was by dicing individual or arrays of VCSELs from whole wafers and placing them into standard laser packages like TO-46 and TO-56 after optimizing the packages for multigigahertz applications [7], [10]. More recently, there has been a growing interest to integrate VCSELs onto another host substrate to realize integrated microsystems. Initial attempts involved usage of conductive epoxies and wire bonds for bonding VCSELs onto the host substrates. Later on, due to the requirement for precise positioning ($\sim$ 2–3-μm accuracy [11]) of VCSELs for improved optical coupling to subsequent optical elements like the multimode fiber (MMF), etc., flip-chip bonding has been used for packaging both single laser diodes [12] as well as VCSEL arrays [2], [13] onto host substrates. However, these packaging techniques render the VCSEL beam emitted perpendicular to the host substrate. With the development of the system-on-a-chip (SoC) concept, there is an interest to have the VCSEL beam emitting parallel to the substrate so that the coupled elements can either be fabricated or assembled on the same chip. Lee and Grodzinski [14] have demonstrated a method to package a VCSEL array with their beams parallel the substrate using sophisticated three-dimensional (3-D) folded microhinges and microspring latches. However, no solution for the VCSEL beam divergence has been proposed, and the kind of electrical interconnects that has been used is unclear.

In many applications, the VCSEL beam needs to be coupled to other optical elements such as optical fibers and photodiodes (PD). VCSELs mounted with microoptic elements have been demonstrated to improve the optical-coupling efficiency [15]. The packaging of such microoptic-element VCSEL arrays requires additional attention. Also, the thermal management is another critical issue as the operating temperature dictates the reliability and the performance of the VCSELs [9]. The package has to provide a low thermal-resistance path.

The goal of this paper is to address the abovementioned challenges using microelectromechanical systems (MEMS) and the ink-jet technology. We first describe low-cost wafer-level microoptic elements for enhanced VCSEL to MMF coupling. We then describe MEMS microclampers and ink-jet printed reflowed solder techniques for reliable and precise positioning of microoptic-element equipped VCSEL die parallel to the substrate beam and low parasitic electrical interconnections.

II. Microoptic Element

The proposed concept of a microoptic element for an improved optical-coupling efficiency is shown in Fig. 1.

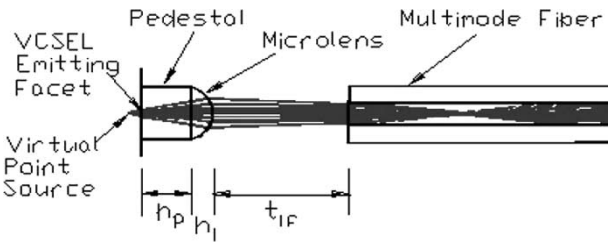

Fig. 1. Concept of the integration of a microoptic element (pedestal and microlens) with a VCSEL for effective light coupling to an MMF.

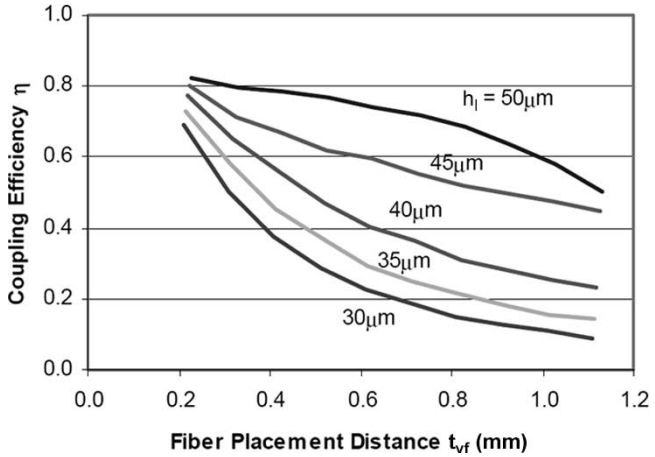

Fig. 2. Coupling efficiency versus axial distance (from the VCSEL emitting facet to the MMF tip) for different lens heights with a pedestal height of 80 μm and a diameter of 120 μm.

The microoptic element consists of ink-jet-printed polymeric microlens on top of the patterned SU-8 (MicroChem Corporation, Newton, MA) photoresist pedestal, which is placed directly on the VCSEL's emitting facet. The cylindrical SU-8 pedestal is characterized by its height h_p, diameter d_l, and index of refraction n_p, which is 1.586 at an 850-nm [16] wavelength. The diameter of the microlens is the same as that of the SU-8 pedestal. The microlens' specification include a diameter d_l, a height h_l, and an index of refraction n_l, which is 1.5037 at 850 nm. The VCSEL output beam is shaped by the microoptic element and coupled into an MMF placed in axis and with a distance t_{lf} from the lens' vertex. It is designed to achieve a high coupling efficiency and to provide a large working space $t_{vf}(t_{vf} = h_p + h_l + t_{lf})$.

Among all parameters, the n_p, n_l, and diameter of the emitting facet of VCSEL d_o; the numerical aperture of the VCSEL emission $\mathrm{NA_{VCSEL}}$; the core diameter of the MMF d_c; and the numerical aperture of the MMF $\mathrm{NA_{MMF}}$ are predetermined. This leaves only the three parameters d_l, h_p, and h_l to be determined. In practice, d_l can only be varied in a small range of 80–120 μm. The upper limit is set by the existing 250-μm-pitch VCSEL-array layout, which has a gold bonding pad of 120-μm diameter. The lower limit is set by the stepwise increment on the lens parameter by the integer number of drops of ink-jet printed polymers. Based on this, 100–120 μm is chosen as the microlens diameter.

In order to find the optimal design of the microoptic element, we investigated the optical-coupling efficiency η as a function of the lens height. Fig. 2 shows the ray tracing simulation results that gives the optical-coupling efficiency η as a function of fiber placement distance t_{vf} by varying the lens height in the range of 30–50 μm for the case of the SU-8 pedestal height of 80 μm and the diameter of the pedestal and the lens of 120 μm. Also, based on the simulation, it has been found that a tall pedestal and a high aspect ratio (height/diameter) of the microlens are desirable. However, both of these geometrical parameters are limited by the fabrication process and materials involved. Using practically achievable values of pedestal height of 100 μm and the lens aspect ratio of 0.5:1, the simulation result showed that the beam is still diverging but it has $\eta > 0.8$ for a t_{vf} of 0.4 mm, which is substantially higher than $\eta < 0.2$ for a diverging beam with no microoptic element at the same t_{vf} due to the divergent nature (30° beam divergence angle) of the VCSEL beam.

Based on the simulation, the microoptic element has been fabricated. The fabrication sequence was started with spin casting and patterning of 100-μm thick SU-8 2075 pedestal array onto the GaAs wafer having a two-dimensional (2-D) array of VCSELs. The fabrication of microlens on top of the SU-8 pedestal was carried out using fast reliable data-driven direct-write polymer ink-jet printing technology [15]. The microlens material, MRXH series, is an in-house (MicroFab Technologies, Inc.) developed 100% solid (solvent free) formulation of prepolymer [15]. Varying the number of drops printed on each pedestal prints microlenses of varying heights. The microlens height variation for a given drop number of polymer was less than 1% over the entire wafer. The polymer stays on the top of the pedestal without flowing down and self-centers due to surface tension. The entire wafer was UV cured and baked to harden the microlens polymer. The wafer was then diced into one-dimesional (1-D) and 2-D arrays of chosen sizes. Fig. 3(a) shows a wafer-level fabricated microoptic element, and Fig. 3(b) shows a diced 4 × 1 VCSEL array with microoptical elements.

Optical losses were measured using the Newport optical meter 1825-C to compare three cases: VCSELs without the microoptic element; VCSELs with an SU-8 pedestal only (no polymer lens); and VCSELs with the microoptic element. Fig. 4(a) shows the dc characteristics of total emitted optical power and also the forward voltage as functions of the driving current of a VCSEL. It is observed that the curves for all the three cases are close to each other, indicating that the presence of the microoptic element does not cause any substantial optical loss.

Fig. 4(b) shows a plot of the measured optical-coupling efficiency for a VCSEL-to-MMF coupling with a varying VCSEL-to-MMF axial distance. A comparison of the optical-coupling efficiency achieved for VCSELs having varying heights of microlenses has been made. The control parameter N is the drop number of the polymer dispensed. Butt coupling is also presented for comparison. $N = 0$ is the case for the SU-8 pedestal without the microlens. $N = 3 \sim 7$ result in a series of lens heights of 25, 28, 33, 36, and 38 μm. At the typical axial working distance of 0.4 mm between the microlens tip

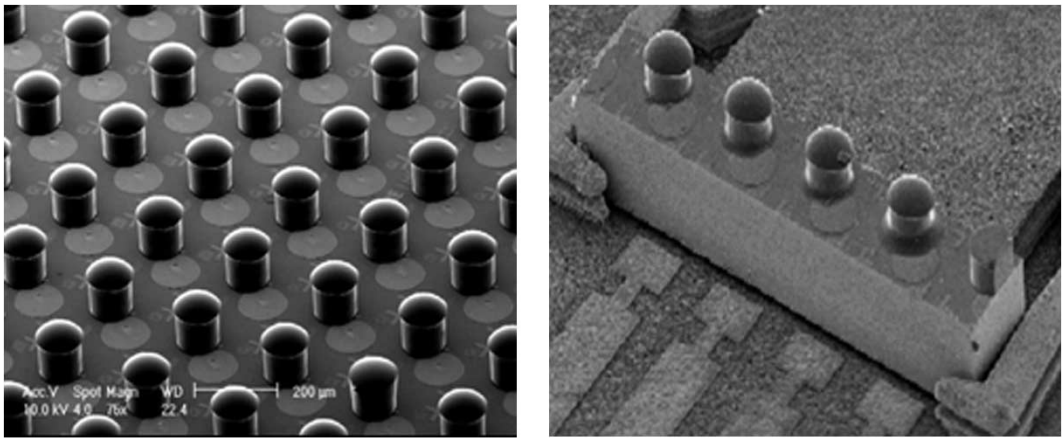

Fig. 3. SEM photomicrographs. (a) Wafer-level fabricated microoptic element array and (b) diced 4×1 VCSEL array.

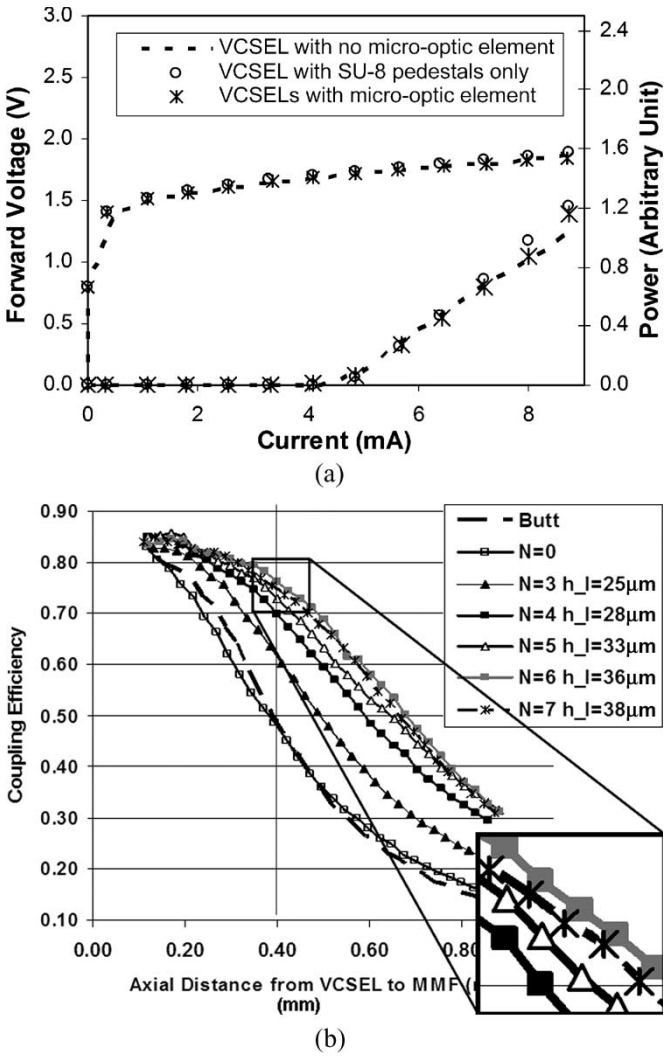

Fig. 4. (a) Measured dc characteristics of VCSELs. (b) Measured coupling efficiency versus axial distance (from the VCSEL emitting facet to the MMF tip) for different lens heights with a pedestal height of 100 μm and a diameter of 120 μm.

and the MMF, the coupling efficiency has increased from about 45% for butt coupling to about 75% due to the presence of the microoptic element.

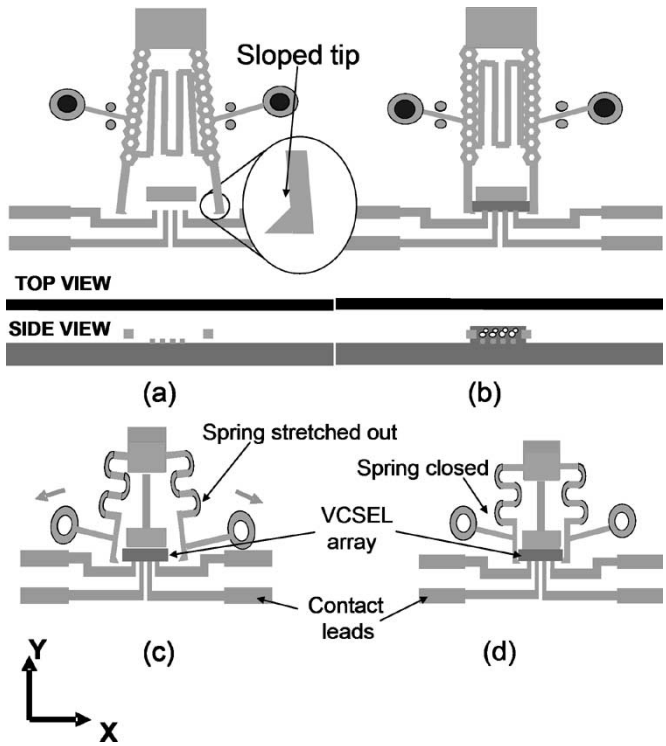

Fig. 5. Mechanical assembly procedures for (a), (b) the type-1 and (c), (d) the type-2 micro clampers.

III. Micro Clampers

In order to provide reliable and precise positioning of VCSEL die onto a substrate, we investigated micro-clamper structures. Fig. 5(a) and (b) shows a type-1 micro clamper, and Fig. 5(c) and (d) shows a type-2 micro clamper. Micro clampers are of a two-layered structure made of electroplated nickel. The first layer is for anchoring as well as for electrical interconnection, and the second layer is a springlike structural layer. The x-direction is defined as the direction perpendicular to the micro clamper arms, and the y-direction is defined as the direction parallel to the arms. Probes are inserted into the ring-like structures attached to each arm and stretched out to open the arms. This opens up a positional window between the arms

TABLE I
MATERIAL PROPERTIES FOR ELECTROPLATED Ni FILM

Parameter	Value
Density	1890 kg/m^3
Young's modulus	180 GPa
Poisson's Ratio	0.31

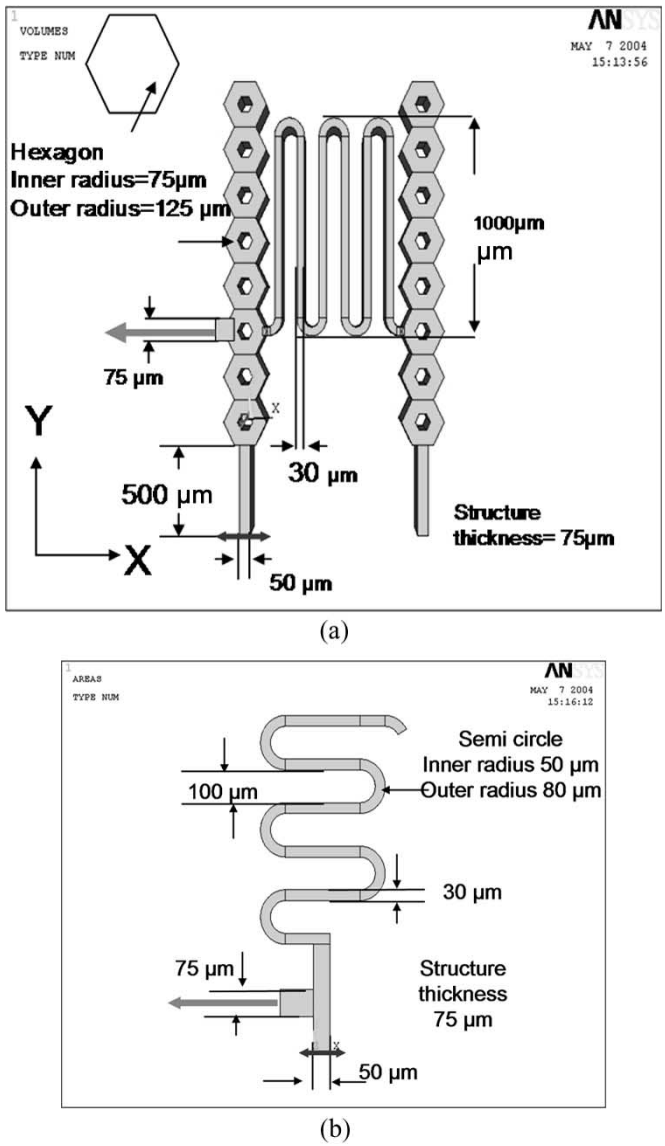

Fig. 6. (a) ANSYS model of a type-1 micro clamper. (b) ANSYS model of the half section of a type-2 micro clamper.

into which a 4×1 VCSEL array is placed. Once the probes are released, the VCSEL-array dies are brought into position. The sloped tip [shown in the inset of Fig. 5(a)] of the type-1 clamper pushes the VCSEL die towards the back wall as the arm closes realizing y-direction alignment. A type-2 clamper has serpentine-shaped beams. Micro clampers' clamping forces are given by $F_x = k_x \cdot \delta x$ and $F_y = k_y \cdot \delta y$, where F_x and F_y are the clamping forces, k_x and k_y are the effective spring constants, and δx and δy are the distances from the rest position in x- and y-directions, respectively. If the spring constant is low, the clamping force may not be sufficient to stably grip the VCSEL die. Based on a simple calculation, frictional forces

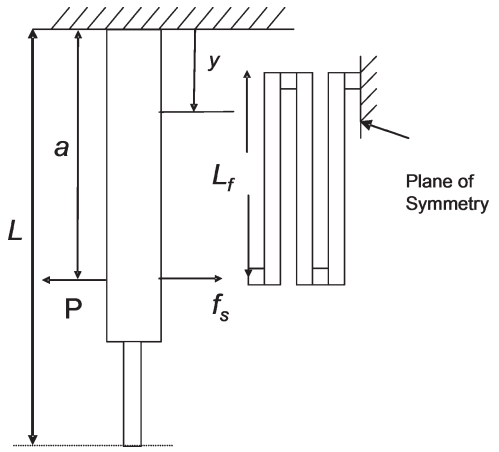

Fig. 7. Approximated model of a type-1 micro clamper used for the analytical calculation.

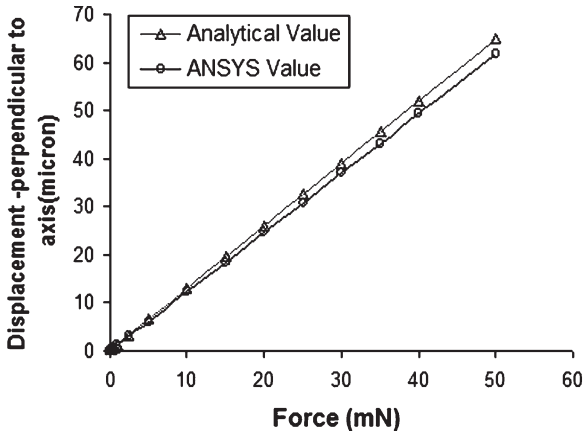

Fig. 8. Comparison of analytical and ANSYS values for the deflection of the clamper arm in the x-direction of the type-1 micro clamper.

were found to be in the order of a few micronewtons. Thus, the clamping force must be greater than few micronewtons in order to position the diced VCSEL with the desired accuracy. On the other hand, if the spring constant is high, the stresses involved during assembly may cause the spring to undergo a plastic deformation.

ANSYS, a commercially available finite-element modeling (FEM) package, has been used for the modeling of these micro-clamper structures. The physical property values for the electroplated nickel used are detailed in Table I [17]. Fig. 6(a) and (b) shows the model parameters used for both type-1 and type-2 micro clampers.

A theoretical modeling has also been carried out for both types. In the theoretical model of the type-1 micro clamper (Fig. 7), hexagonal etch holes were eliminated as they do not contribute much to the beam spring constant and the serpentine-spring short arms are assumed to be straight beams instead of curved ones. The amount of deflection of the type-1 micro clamper at position $y = L$ is given by [18]

$$\delta_L = \frac{(P - f_s)a^2(3L - a)}{6EI_{\text{ave}}} \tag{1}$$

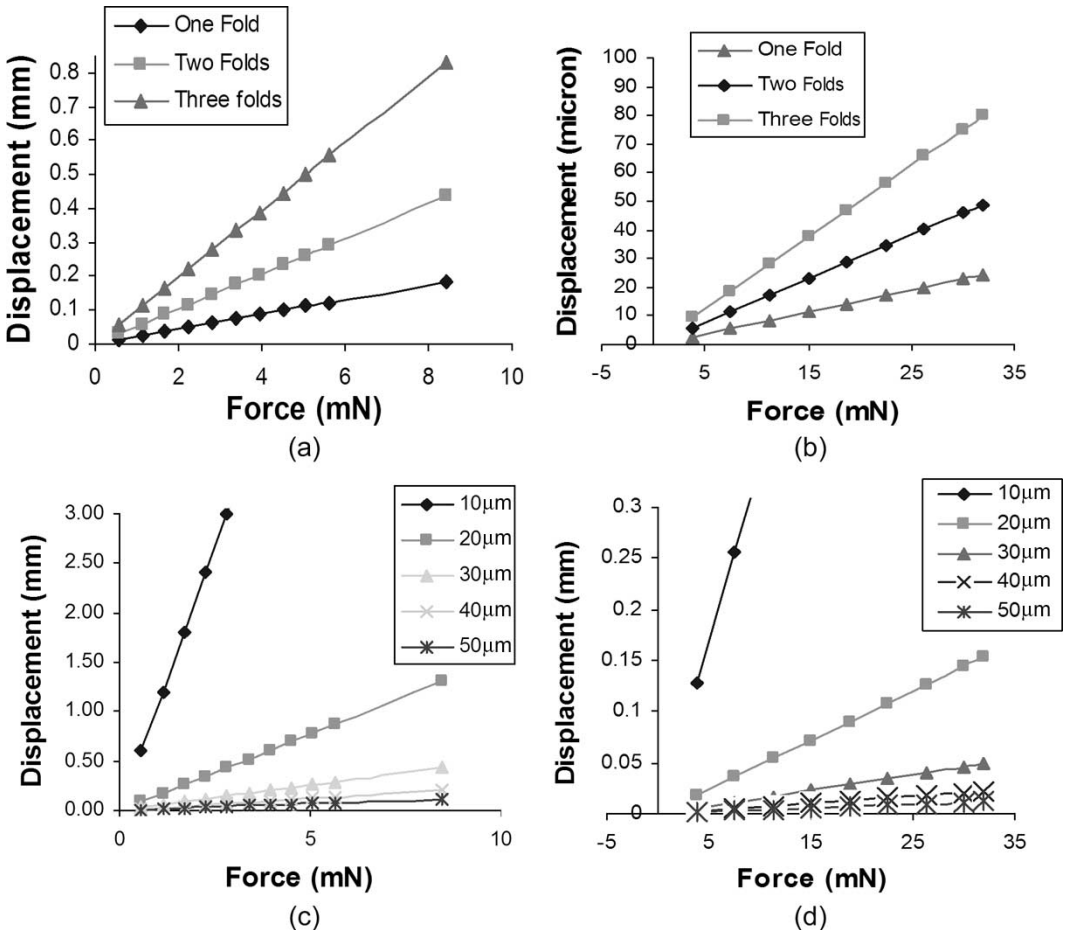

Fig. 9. Type-2 micro-clamper clamping forces with varying parameters. (a) Variation of the spring constant in the x-direction with varying numbers of folds. (b) Variation of the spring constant in y-direction with varying numbers of folds. (c) Variation of the spring constant in x-direction with varying widths of beams. (d) Variation of the spring constant in y-direction with varying widths of beams.

where $f_{\rm s}$ is the force due to the serpentine spring attached to the cantilever beam, P is the applied load, E is the Young's modulus, a is the distance from the anchor point of the clamper arm to the point where load P is applied, and $I_{\rm ave}$ is the average moment of inertia of the cantilever beam. The force $f_{\rm s}$ exerted by the serpentine part is given by [19]

$$f_{\rm s} = K_{\rm fold}\delta_{\rm a} = \frac{12EI_{\rm f}}{L_{\rm f}^3}\frac{1}{3}\delta_{\rm a} \tag{2}$$

where $I_{\rm f}$ is the moment of inertia, $\delta_{\rm a}$ is the deflection of the clamper arm at the point where load P is applied, $L_{\rm f}$ is the length of one of the cantilever beams forming the folded serpentine spring, and $k_{\rm fold}$ is the spring constant of the serpentine spring, which can be solved with an assumption that the spring is composed of folded flexures with three guided cantilever beams. By putting (2) into (1), the force due to the serpentine spring is given by

$$f_{\rm s} = \frac{K_{\rm fold}Pa^3}{3EI_{\rm ave} + K_{\rm fold}a^3}. \tag{3}$$

By putting (3) into (1), we derive the amount of clamper arm deflection δ_L at the end of the micro-clamper arm as a function of applied load P as

$$\frac{\delta_L}{P} = \frac{\left(1 - \frac{K_{\rm fold}a^3}{3EI_{\rm ave}+K_{\rm fold}a^3}\right)a^3(3L-a)}{6EI_{\rm ave}}. \tag{4}$$

The theoretical-modeling and the ANSYS-modeling results were compared, and a good agreement between the results were shown (Fig. 8).

ANSYS simulations for the type-2 micro-clamper serpentine-spring arm, of which mean dimensions are shown in Fig. 6(b), have been done to study the variations of its spring constant with the beam thickness and the number of folds. The variations of the spring constant in the x- and the y-directions for a varying number of folds are shown in Fig. 9(a) and (b), respectively, while the variations of the spring constant in the x- and the y-directions for a varying beam width are plotted in Fig. 9(c) and (d), respectively. Based on these results, triple-folded springs with 30-μm beam widths were chosen. The resulting clamping force for the type-2 micro clamper in the x-direction is 500 μN and 1 mN in the y-direction. The resulting clamping force in the x-direction for the type-1 micro clamper based on a similar analysis is 750 μN.

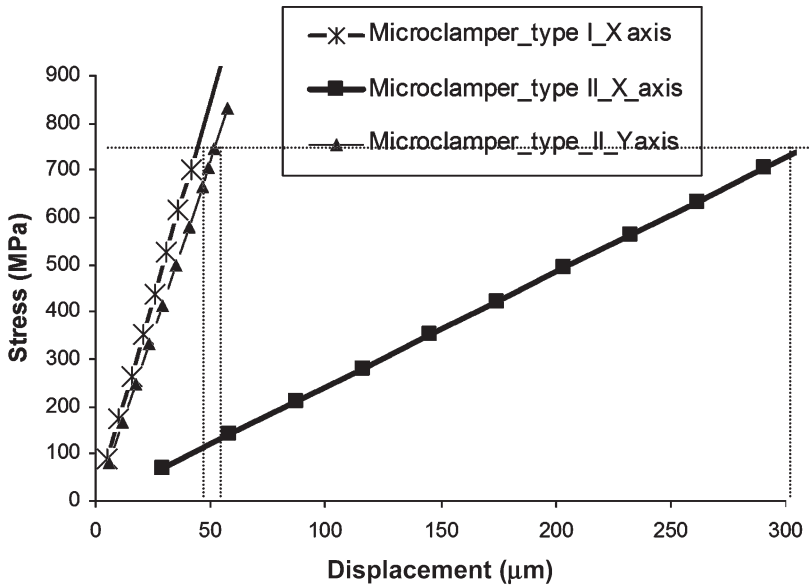

Fig. 10. Von Mises stresses in the arms of the springs with varying tip displacements. Corresponding displacements are marked out for a yield stress of 750 MPa.

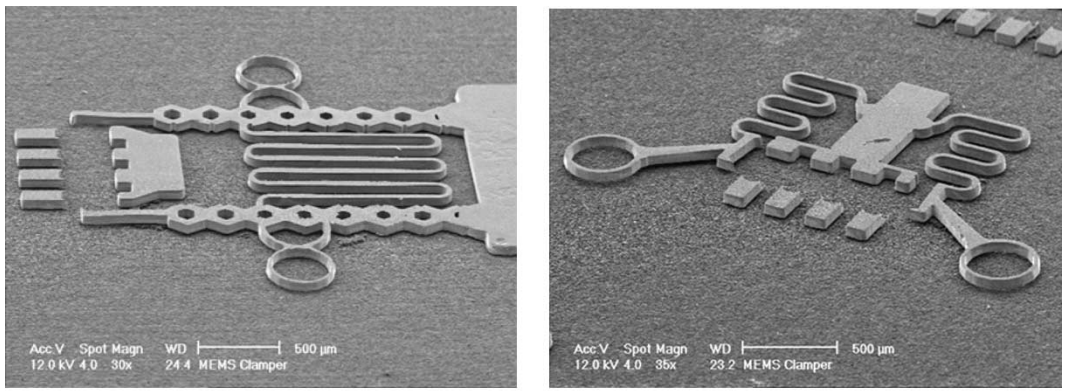

Fig. 11. SEM pictures. (a) Type-1 micro clamper structure. (b) Type-2 micro clamper structure.

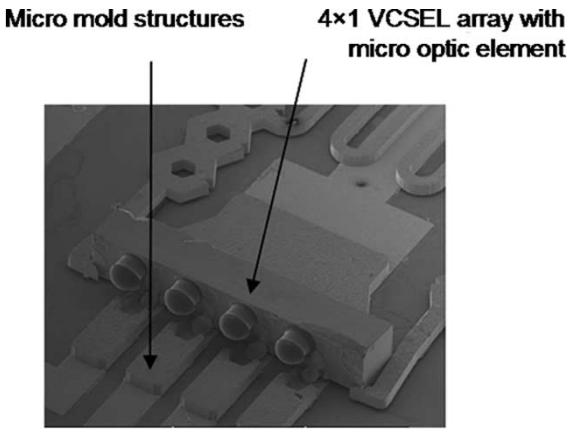

Fig. 12. A 4 × 1 VCSEL array held in position by a type-1 micro clamper.

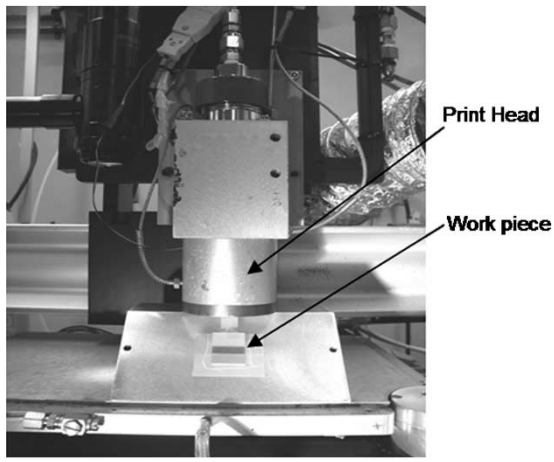

Fig. 13. Solder-jet head used for solder printing.

In order to find the elastic range of movement of the spring, a simulation was carried out to determine the stresses involved in the spring for various displacements. For the chosen electroplating condition of 7 mA/cm^2 for the fabrication of these structures, the yield stress is approximately 750 MPa [17]. Fig. 10 shows the maximum Von Mises stresses in spring arms for various displacements for both type-1 and type-2 micro

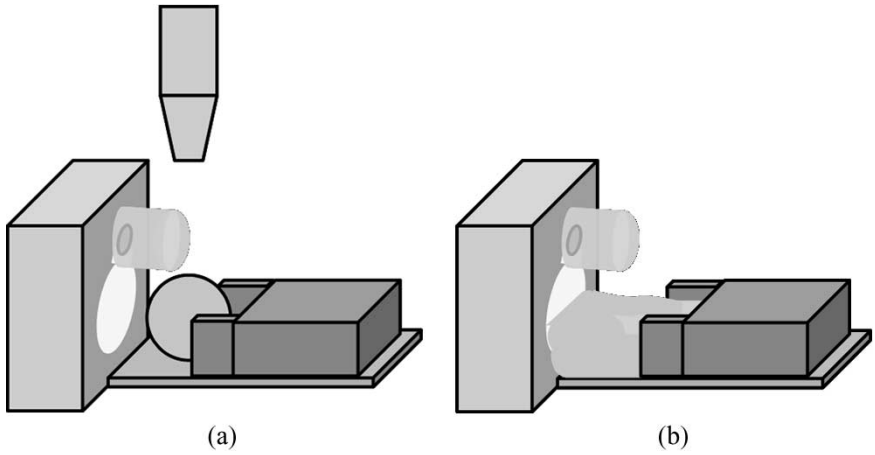

Fig. 14. Schematic diagrams. (a) Solder ball printed into the micromold structure. (b) Electrical interconnection established after reflow.

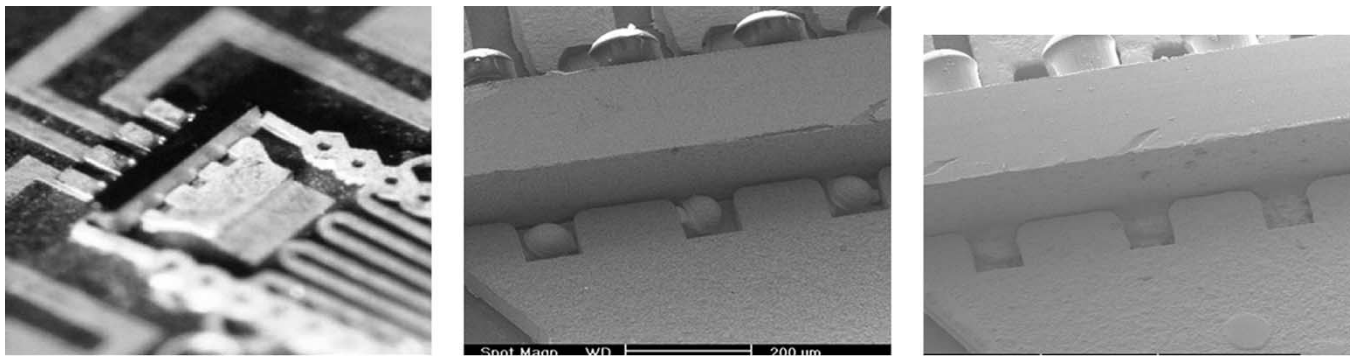

Fig. 15. Backside view of a 4×1 VCSEL array held by a micro clamper (a) before solder printing, (b) after printing, and (c) after reflow.

clampers. The positional window dimensions for the serpentine spring are about 1600 μm in x-axis and about 275 μm in the y-axis to fit in a VCSEL array of which the dimensions are 1000 μm by 225 μm. For the type-1 micro clamper, the positional window is about 275 μm in x-direction. This ensures that the spring movement stays in the elastic range of operation and an accurate positioning for the VCSEL array is obtained.

The fabrication of the micro clampers and micromolds was started with a sputter deposition of a triple layer of metals (Cr/Cu/Cr, 100/2,000/150 Å) on top of a substrate. Various types of substrates including RF-friendly alumina, oxidized silicon wafer, and glass with varying degrees of surface roughness were used. SU-8 2010 was spin casted and patterned using conventional UV lithography to create a 15-μm thick SU-8 mold. Nickel electroplating was carried out through the SU-8 mold approximately up to 13-μm, and the last 2 μm was electroplated with gold for the contact leads and anchor pads. Another layer of the metallic seed layer was deposited; SU-8 2075 was spin casted and patterned to have an 80-μm thick SU-8 mold for the structural layer. Nickel electroplating was carried out to create the metallic micro clamper structures. The SU-8 mold layers were removed by O_2/CF_4 plasma, and the metallic seed layers were removed by chemical wet etch techniques to create the suspended metallic micro clamper structures. Fig. 11(a) and (b) shows scanning electron microscopy (SEM) images of the fabricated type-1 and type-2 micro clampers on an alumina substrate.

The mounting of the VCSEL onto the micro clamper was done manually using a probe station. Probes were inserted into the rings attached to the clamper arms and stretched to hold the arms open while the VCSEL array was placed between them. Fig. 12 shows a 4×1 VCSEL array with an integrated microoptic element clamped by a micro clamper.

To obtain an electrical interconnect to the VCSEL die, a Microfab Technologies Solderjet station (Fig. 13) was used. The printhead (piezoelectric jetting device and liquid solder reservoir) was operated at temperatures above 200 °C for a eutectic 63Sn/37Pb alloy. An N_2 coflow was applied at the dispensing nozzle to prevent the molten solder from oxidation. Reflow was then carried out at 200-°C in a forming gas environment for about 3 min to complete the electrical connection. Fig. 14(a) and (b) shows the micromold structure in which the solder was printed and reflowed to fill up the mold. A similar mold pattern was designed to connect the cathode metallization on the backside of the VSCEL die with the Cu lead on the MEMS substrate. Fig. 15 shows the backside ground contact before printing, after printing, and after reflow.

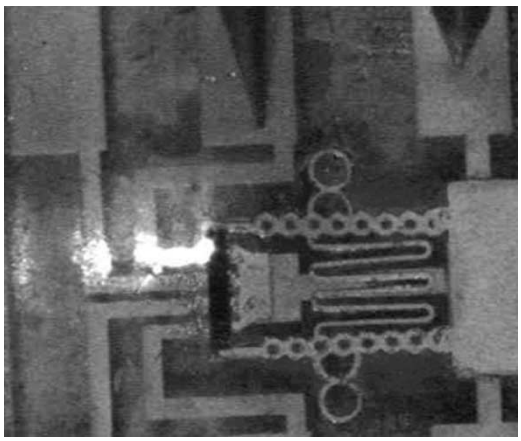

Fig. 16. Fully assembled VCSEL array with one of the VCSELs fired on and emitting 850-nm laser as seen by an infrared-sensitive camera.

Four $\times$ 1 VCSEL arrays with microoptic elements have been reliably mounted into both type-1 and type-2 micro clampers and electrically interconnected using a reflowed solder in micromolds on various substrates. The VCSEL arrays stayed stably clamped all through the solder printing and reflow process. The positional accuracy measured was within 3 μm of the expected position for all the assembled samples. It has been observed that the positioning accuracy of the VCSEL array was primarily governed by the restoring force of the micro clamper and not by the substrate roughness. The measured alignment error includes the alignment error created by the fabrication process between the micro clampers and the patterned conductor lines on the substrate. The assembled VCSEL has been tested at the maximum specified operating voltage of 12 V for several hours. Fig. 16 shows one of the VCSELs in the 4 $\times$ 1 array being fired.

The VCSEL performance reliability is highly dependent on the operating temperature. The average lifetime of a VCSEL is expected to improve by a factor of two for every 10-°C decrease in the junction temperature [9]. As the process is substrate independent, substrates with high thermal conductivities such as aluminum nitride can be used. In addition, the electroplated nickel present in close proximity to the VCSEL array on three sides also help in the heat dissipation. VCSELs are designed to perform at high speeds in excess of 10 GHz. Improper electrical packaging causes the degradation of electrical signals at high frequencies. The inherent capacitive and inductive parasitics associated with many electronic interconnect-like wire bonds are one of the major contributors to this signal degradation. Although it was not measured, it is expected that eliminating the wire bond with a solder interconnect would greatly reduce parasitic losses.

IV. Conclusion

We have successfully demonstrated a novel approach to VCSEL packaging using MEMS and the ink-jet technology. For the improvement of a VCSEL to an MMF coupling, microoptic elements were designed and fabricated using an SU-8 pedestal with a UV-curable polymer lens on top. A two-layered metallic MEMS process was used to build micro clampers and micromolds for the mechanical and electrical assembly of 4 $\times$ 1 VCSEL arrays. Since this new approach is a relatively simple and substrate-independent process, it would give an alternative solution to many challenging issues in VCSEL packaging. Furthermore, a similar approach with an integration of MEMS actuators will realize an in-plane moveable light source and a microoptic element, which may be used in a varied range of optical bench-on-chip applications.

Acknowledgment

The authors would like to thank M. Boldman, V. Shah, and R. Hoenigman of MicroFab Technologies Inc. for their support on the ink-jet printing of solder and optical polymer and the members of the Micro/Nano Device and Systems (MiNDS) Laboratory and Clean Room Staff at the University of Texas at Dallas (UTD) for their support.

References

[1] J. A. Tatum, "Packaging flexibility propels VCSELs beyond telecommunications," *Laser Focus World*, vol. 36, no. 4, pp. 131–136, Apr. 2000.

[2] J. J. Liu, K. A. Olver, M. T. Lara, T. Taylor, W. Chang, and S. Horst, "High yield flip-chip bonding and packaging of low-threshold VCSEL arrays on sapphire substrates," *IEEE Trans. Compon. Packag. Technol.*, vol. 26, no. 3, pp. 548–553, Sep. 2003.

[3] Y. Ishii, N. Tanaka, T. Sakamoto, and H. Takahara, "Fully SMT-compatible optical-I/O package with microlens array interface," *J. Lightw. Technol.*, vol. 21, no. 1, pp. 275–280, Jan. 2003.

[4] T. Chen, A. K. Nallani, J. B. Lee, D. J. Hayes, and D. B. Wallace, "Inkjet printing for optical/electrical Interfacing of VCSEL and PD arrays," in *Proc. IMAPS Int. Symp. Microelectronics Processing*, Boston, MA, 2003, pp. 864–868.

[5] S. Kawai, "Parallel micro-optics for interconnections based on VCSEL arrays and their Jisso technologies," *Opt. Eng.*, vol. 43, no. 5, pp. 1018–1021, May 2004.

[6] K.-M. Chu, J.-S. Lee, H. S. Cho, B. S. Rho, H.-H. Park, and D. Y. Jeon, "Characteristics of indium bump for flip-chip bonding used in polymeric-waveguide-integrated optical interconnection systems," *Jpn. J. Appl. Phys.*, vol. 43, no. 8B, pp. 5922–5927, 2004.

[7] S. H. Hall, W. L. Walters, L. F. Mattson, G. J. Fokken, and B. K. Gilbert, "VCSEL electrical packaging analysis and design guidelines for multi-GHz applications," *IEEE Trans. Compon., Packag., Manuf. Technol. B*, vol. 20, no. 3, pp. 191–201, Aug. 1997.

[8] G. J. Fokken, W. L. Walters, L. F. Mattson, and B. K. Gilbert, "Low-cost, multi-Ghz electrical packaging for serial optoelectronic links utilizing vertical cavity surface emitting lasers," *IEEE Trans. Adv. Packag.*, vol. 23, no. 1, pp. 42–54, Feb. 2000.

[9] Y. C. Lee, S. E. Swirhun, W. S. Fu, T. A. Keyser, J. L. Jewell, and W. E. Quinn, "Thermal management of VCSEL-based optoelectronic modules," *IEEE Trans. Compon., Packag., Manuf. Technol. B*, vol. 19, no. 3, pp. 540–547, Aug. 1996.

[10] K. H. Gulden, S. Eithel, H. P. Gauggel, R. Hovel, M. Moser, and H. P. Zappe, "VCSEL array technology for optical interconnects," in *Proc. LEOS'99, 12th Annual Meeting*, 1999, vol. 2, pp. 760–761.

[11] Y. Ishii, S. Koike, Y. Arai, and Y. Ando, "Hybrid integration of polymer microlens with VCSEL using drop-on-demand technique," in *Proc. SPIE*, San Jose, CA, 2000, vol. 3952, pp. 364–370.

[12] T. Hashimoto, Y. Nakasuga, Y. Yamada, H. Terui, M. Yanagisawa, K. Moriwaki, Y. Suzaki, Y. Tohmori, Y. Sakai, and H. Okamoto, "Hybrid integration of spot-size converted laser diode on planar lightwave circuit platform by passive alignment technique," *IEEE Photon. Technol. Lett.*, vol. 8, no. 11, pp. 1504–1506, Nov. 1996.

[13] A. V. Krishnamoorthy, L. M. F. Chirovsky, S. W. Hobson, R. E. Leibengath, S. P. Hui, G. J. Zydzik, K. W. Goossen, J. D. Wynn, B. J. Tseng, J. Lopata, J. A. Walker, J. E. Cunningham, and L. A. D'Asaro, "Vertical-cavity surface-emitting lasers flip-chip bonded to gigabit-per-second CMOS circuits," *IEEE Photon. Technol. Lett.*, vol. 11, no. 1, pp. 128–130, Jan. 1999.

[14] H. C. Lee and P. Grodzinski, "Passively aligned hybrid integration of 8×1 micromachined micro-Fresnel lens arrays and 8×1 vertical-cavity surface-emitting laser arrays for free-space optical interconnect," *IEEE Photon. Technol. Lett.*, vol. 7, no. 9, pp. 1031–1033, Sep. 1995.
[15] T. Chen, W. Cox, D. Lenhard, and D. Hayes, "Microjet printing of high-precision microlens array for packaging of fiber optic components," in *Proc. SPIE—Int. Soc. Opt. Eng.*, San Jose, CA, 2002, vol. 4652, pp. 136–141.
[16] A. Borreman, S. Musa, A. A. M. Kok, M. B. J. Diemeer, and A. Driessen, "Fabrication of polymeric multimode waveguides and devices in SU-8 photoresist using selective polymerization," in *Proc. Symp. IEEE/LEOS Benelux Chapter*, Amsterdam, The Netherlands, 2002, pp. 83–86.
[17] T. Fritz, H. S. Cho, K. J. Hemker, W. Mokwa, and U. Schnakenberg, "Characterization of electroplated nickel," *Microsyst. Technol.*, vol. 9, no. 1–2, pp. 87–91, Nov. 2002.
[18] J. M. Gere and S. N. Timoshenko, *Mechanics of Materials*, 4th ed. Boston, MA: PWS-Kent, 1997.
[19] G. K. Fedder, "Simulation of microelectromechanical systems," Ph.D. dissertation, Dept. Elect. Eng. Comput. Sci., Univ. California, Berkeley, 1994.

Arun Kumar Nallani was born in Hyderabad, India, in 1979. He received the B.E. degree in electronics and communication engineering from Osmania University, Hyderabad, in 2000 and the M.S. and Ph.D. degrees in electrical engineering from the University of Texas at Dallas (UTD), Richardson, in 2002 and 2005, respectively. The topic of his Ph.D. thesis was "Microelectromechanical Systems (MEMS) for Heterogeneous Integration of Microsystems," in which microoptical, micro-fluidic, and RF microsystem integration is realized using the MEMS technology.

From June 2003 to May 2005, he was a Research Intern at MicroFab Technologies, Plano, TX. He is currently with Intel Corporation, Chandler, AZ, as a Packaging Engineer in the Assembly Technology Development (ATD) Group.

Ting Chen (M'96), photograph and biography not available at the time of publication.

Donald J. Hayes, photograph and biography not available at the time of publication.

Woo-Seong Che received the B.E. degree from Hanyang University, Seoul, Korea, and the M.S. and Ph.D. degrees from Korea Advanced Institute of Science and Technology (KAIST), Daejon, Korea, in 1984, 1989, and 1997, respectively, all in mechanical engineering.

From 1995 to 1998, he was a Senior Researcher at Mando Central Research Center, Gyunggido, Korea. He is currently an Associate Professor in the Department of Mechatronics Engineering, Tongmyong University of Information Technology, Busan, Korea. His research interests include microelectromechanical systems (MEMS) device design, sensor design for automobile, and computer aided engineering (CAE) for MEMS.

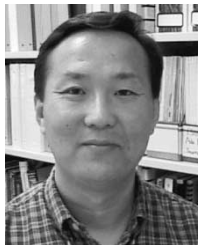

Jeong-Bong Lee (S'92–M'97) received the B.S. degree in electronics engineering from Hanyang University, Seoul, Korea, in 1986 and the M.S. and Ph.D. degrees in electrical engineering from Georgia Institute of Technology, Atlanta, in 1993 and 1997, respectively.

In 1999, he joined Louisiana State University (LSU), Baton Rouge, as an Assistant Professor. Then, in May 2001, he moved to the University of Texas at Dallas (UTD), Richardson, where he is currently a tenured Associate Professor in the Department of Electrical Engineering. His current research interests include microelectromechanical systems (MEMS)/ nanoelectromechanical systems (NEMS) for packaging, RF, Bio-MEMS, and photonic applications.

Prof. Lee is a recipient of the National Science Foundation (NSF) Career Award in 2001.